Vietnam Journal of Earth Sciences, 46(2), 252-271, https://doi.org/ 10.15625/2615-9783/20274

Vietnam Journal of Earth Sciences
https://vjs.ac.vn/index.php/jse

Petrological and geochemical characteristics of the Low- and High-Hf Nam Meng dioritoid, northwest Vietnam: Implication for the mantle partial melting, mixing, and magmatic differentiation

Tuan-Anh Tran[1], Can Pham-Ngoc[1*], Nguyen Hoang[1], Vu Hoang Ly[1], Ngo Thi Huong[1], Tran Quoc Cong[1], Pham Thi Phuong Lien[1], Tran Trong Hoa[1], Vuong Bui Thi Sinh[1], Pham Thanh Thuy[2]

[1]*Institute of Geological Sciences, Vietnam Academy of Science and Technology, Hanoi, Vietnam*
[2]*Faculty of Geology, University of Science, Ho Chi Minh City, Vietnam*

Received 07 November 2023; Received in revised form 12 December 2023; Accepted 06 March 2024

ABSTRACT

This paper investigated the petrological, elemental, and isotope geochemical characteristics of the Nam Meng dioritoid to clarify the magma source and process. The Nam Meng massif comprises large amounts of dioritoids (gabbro-diorite and quartz diorite) and lesser amounts of granitoids (granodiorite and granite). The Nam Meng gabbro-diorite is a porphyritic texture with fine-grained plagioclase, amphibole, K-feldspar, and phenocryst biotite. The Nam Meng quartz diorite comprises coarse-grained plagioclase, amphibole, biotite, quartz, and K-feldspar. The Nam Meng gabbro-diorite contains higher plagioclase and lower biotite and quartz than the Nam Meng quartz diorite. The variation in petrography and mineralogy with the negative correlation between SiO_2 contents with Al_2O_3, MgO, Al_2O_3 + MgO, T-Fe_2O_3, and CaO contents suggest a magmatic differentiation process. All the Nam Meng dioritoids have low ACNK (mostly less than 1.0), total alkaline ($Na_2O + K_2O \leq 6$ wt.%) with $Na_2O/K_2O \geq 1$, and negative anomalies of Ta, Nb, and Ti. Combined with the U-Pb zircon age of 290 Ma (Hieu et al. (2017), the Nam Meng dioritoid is thought to be an I-type granitic rock formed in the subduction stage of the Indosinian amalgamation event. The low La/Yb ratios (1.14-3.21) suggest that the mantle wedge that was melted to form the Nam Meng magma had a spinel peridotite composition. The $\varepsilon_{Nd\ (290\ Ma)}$ of the Nam Meng dioritoid is close to bulk earth silicate at 290 Ma (-4.43 to 2.34). The $^{87}Sr/^{86}Sr_{\ (290\ Ma)}$ of the Nam Meng dioritoid varies in a wide range from low to intermediate (0.6987 to 0.7088), and the calculated Nd model age of the Nam Meng dioritoid is 1,258 ± 47 Ma. The Sr and Nd isotope data suggest that the Nam Meng spinel peridotite was a result of mixing between an ancient ocean crust, EM1, and EM2 that occurred in a paleo-subduction zone at Meso-Neoproterozoic Rodinia supercycle. The Hf contents of the low-Hf and high-Hf Nam Meng dioritoid series are 0.38-1.02 and 2.60-8.08, respectively. The LILE/Hf and HSFE/Hf ratios in the low-Hf Nam Meng dioritoids are high and have a strongly negative correlation with Hf. On the other hand, those ratios in the high-Hf Nam Meng dioritoids are low and have a weakly negative correlation with Hf. The Hf contents positively correlate with the degree of partial melting of the mantle wedge in the subduction zone. Therefore, the low Hf, high LILE/Hf, and HSFE/Hf ratios of the Nam Meng dioritoids could be derived from a low degree of partial melting of the mantle wedge. In contrast, the high Hf, low LILE/Hf, and HSFE/Hf ratios of the Nam Meng dioritoids could be produced by a high degree of partial melting of the mantle wedge.

Keywords: Nam Meng dioritoid, Indosinian subduction, magma origin, partial melting, Hf anomaly.

1. Introduction

The Dien Bien complex (or Dien Bien Phu series) includes Nam Meng, Nam Po, Nam Hon, Muong Tung, and Nam Rom massifs (and numerous small satellite massifs) distributed along the Dien Bien - Lai Chau and Song Ma faults (Fig. 1a; Izokh, 1971;

*Corresponding author, Email: canpn87@gmail.com

Nguyen, 1977). The magmas of the Dien Bien complex vary from gabbro-diorite to leucocratic granite. Early studies of the petrography and major oxides suggested that the Dien Bien intrusive rocks were solidified at a multi-stage under magmatic differentiation in a syn-collision environment (Izokh, 1971; Tran, 1994). Ar-Ar biotite ages of the Nam Meng, Nam Hon, and Nam Rom intrusive rocks (Izokh, 1971) are 235-255, 233, and 252-266 Ma, respectively.

Recent studies about the U-Pb zircon ages suggest that the Nam Meng and Nam Po intrusive rocks differ from the rest of the Dien Bien complex. The Nam Meng intrusive rocks consist of large amounts of dioritoid (gabbro-diorite and quartz diorite) with small amounts of granitoid (granodiorite and granite) (Fig. 2; Tran, 1994). The gabbro-diorite and granodiorite of the Nam Meng massif were formed at 281-276 Ma (Liu et al., 2012) and 296-289 Ma (Hieu et al., 2017), respectively. Quartz diorite and granodiorite of the Nam Po massif were formed at 281 and 277 Ma, respectively (Hieu, 2017). On the other hand, the ages of the Nam Rom intrusive rocks are 244-231 Ma (Hieu et al., 2017, 2019) and 230-225 Ma (Roger et al., 2014; Tran et al., 2022). This age evidence led to a new conclusion that the Nam Meng and Nam Po intrusive rocks were formed at the early stage of Indonesian subduction at 290-280 Ma while the Nam Rom intrusive rocks were formed at the post-collision at 244-225 Ma (Hieu et al., 2019; Tran et al., 2022). Initial studies about the geochemical characteristics of trace elements and Sr and Nd isotopes suggested that Nam Meng gabbro-diorite was derived from mantle-crustal interaction (Liu et al., 2012) or mantle-derived with minor input of crustal material (Tran et al., 2022) and Nam Po quartz diorite and granodiorite was derived from magma that melted from Neoproterozoic ocean island basalt (OIB; Hieu, 2017).

In this paper, whole-rock chemistry and Sr and Nd isotopes of eighteen samples of the Nam Meng dioritoid were studied to clarify the origin and evolution of magma. The results suggest two series in the Nam Meng dioritoid: low-Hf and high-Hf. The former has low Hf contents with negative Hf anomalies. The latter has high Hf contents with no or positive Hf anomalies. They were formed from magmas at different degrees of partial mantle melting.

2. Sampling and analytical methods

2.1. Sampling

The Nam Meng massif is elongated from northwest to southeast (Fig. 1b) at 6 km width and 20 km length. Nineteen samples were collected along the northwest to southeast section. Among them, there were 12 quartz diorite and 7 gabbro-diorite. The Nam Meng quartz diorite is leucocratic granular medium-grained (Figs. 1c, d). The Nam Meng gabbro-diorite consists of menalocratic porphyry fine-grained and mesocratic granular medium-grained. The Nam Meng menalocratic gabbrodiorite occurs as an enclave in the quart diorite and mesocratic gabbrodiorite. The sizes of the enclaves range from several centimeters to several meters. About 200 g of each sample was pulverized for chemical analysis.

2.2. Analytical methods

The thin section was prepared and observed at the Institute of Geological Sciences, Vietnam Academy of Science and Technology (IGS-VAST) using a Zeiss Primotech polarized microscope. The photomicrograph of the thin section was taken by a CCD (Charge Couple Device) camera attached to the microscope.

A Bruker S4 X-ray fluorescence determined the major oxides at the IGS-VAST. The calibration line was composed of a set of Japanese rock standards.

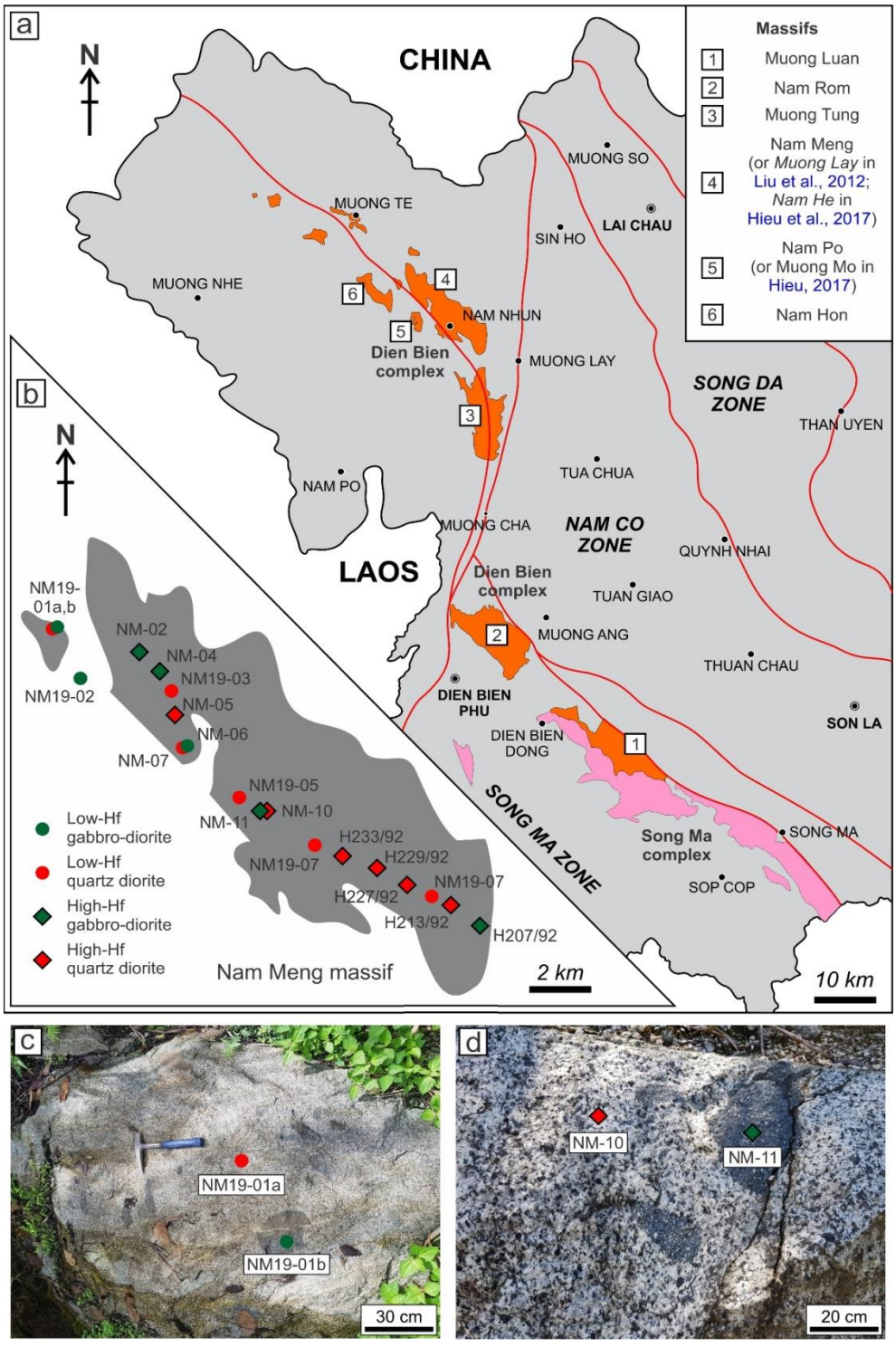

Figure 1. a - Distribution of intrusive massifs of the Dien Bien and Song Ma complexes in northwest Vietnam; b - Sample locations in the Nam Meng massif; c and d - outcrop photographs of the Nam Meng dioritoid. Redrawn from Bui et al. (2005), Phan et al. (2005), and Tran et al. (2005a, b)

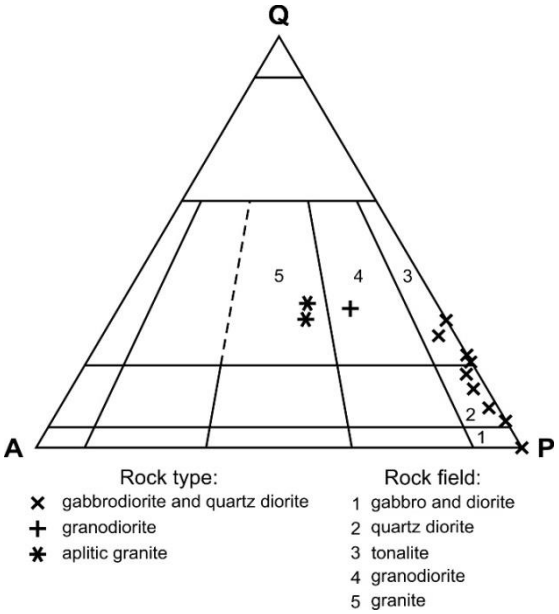

Figure 2. QAP classification diagram of the Nam Meng intrusive rocks (Tran, 1994)

Solutions for the trace elements and isotope analysis were prepared in IGS-VAST. About 50 mg of sample powder was digested by a mixture of condensed HNO_3 and HF at 135°C for 48 hours in a Teflon container. The digested sample evaporated at 145°C for 90 minutes. Then, the sample was cleaned by adding 1 ml HNO_3 and evaporating again. This step is repeated several times until the residue changes to brownish yellow. The sample was digested again in 1 ml condensed HCl at 100°C for 15 minutes. After that, 5-7 ml of ultrapure water is added and evaporated until dry. A part of the digested sample is diluted by an HNO_3 2M to a 0.3M solution for trace elements analysis by a Q-ICP-MS at Ryukyu University, Japan.

Another part of the digested sample was used to isolate the Sr and Nd for the isotopic analysis. The solution is added to the Sr and Nd columns and collected by the HCl and HNO_3. The collected solution is evaporated to remove all HCl. Then, the sample is diluted to an HNO_3 2% for the measurement using a Neptune Plus MC-ICPMS at Ryukyu University.

3. Results

3.1. Petrographical characteristics of the Nam Meng dioritoid

The Nam Meng gabbro-diorite is a porphyritic texture with fine-grained (less than 400 μm in diameter) plagioclase, amphibole, and K-felspar and phenocrystal biotite (greater than 1 mm in diameter). It comprises more than 65% plagioclase, 20-30% amphibolite, less than 5% biotite, quartz, and less than 2% K-felspar. The gabbro-diorite amphibole is pale greenish to dark greenish, anhedral to subhedral crystal. It occurs as a granular grain or inclusion in the plagioclase. The gabbro-diorite biotite is a pale greenish, euhedral crystal replaced by amphibole and plagioclase (Figs. 3a, b, e, f).

The Nam Meng quartz diorite is granular and coarse-grained. The size of the crystal reaches several mm in diameter. It comprises more significant amounts of plagioclase (40-60%) and amphibole (10-35%), lesser amounts of biotite (5-15%) and quartz (10-20%), and a small amount of K-feldspar (less than 2%). The quartz diorite amphibole is subhedral brownish-green color. The quartz diorite plagioclase is a tabular twining crystal. Amphibole and plagioclase are replaced by K-feldspar and quartz, smaller and anhedral crystals (Figs. 3c, d, g, h).

Based on the observations, the low-Hf and high-Hf series have no significant differences in petrographical characteristics. The Nam Meng quartz diorite is larger-grained and comprises more biotite and quartz than the Nam Meng gabbro-diorite.

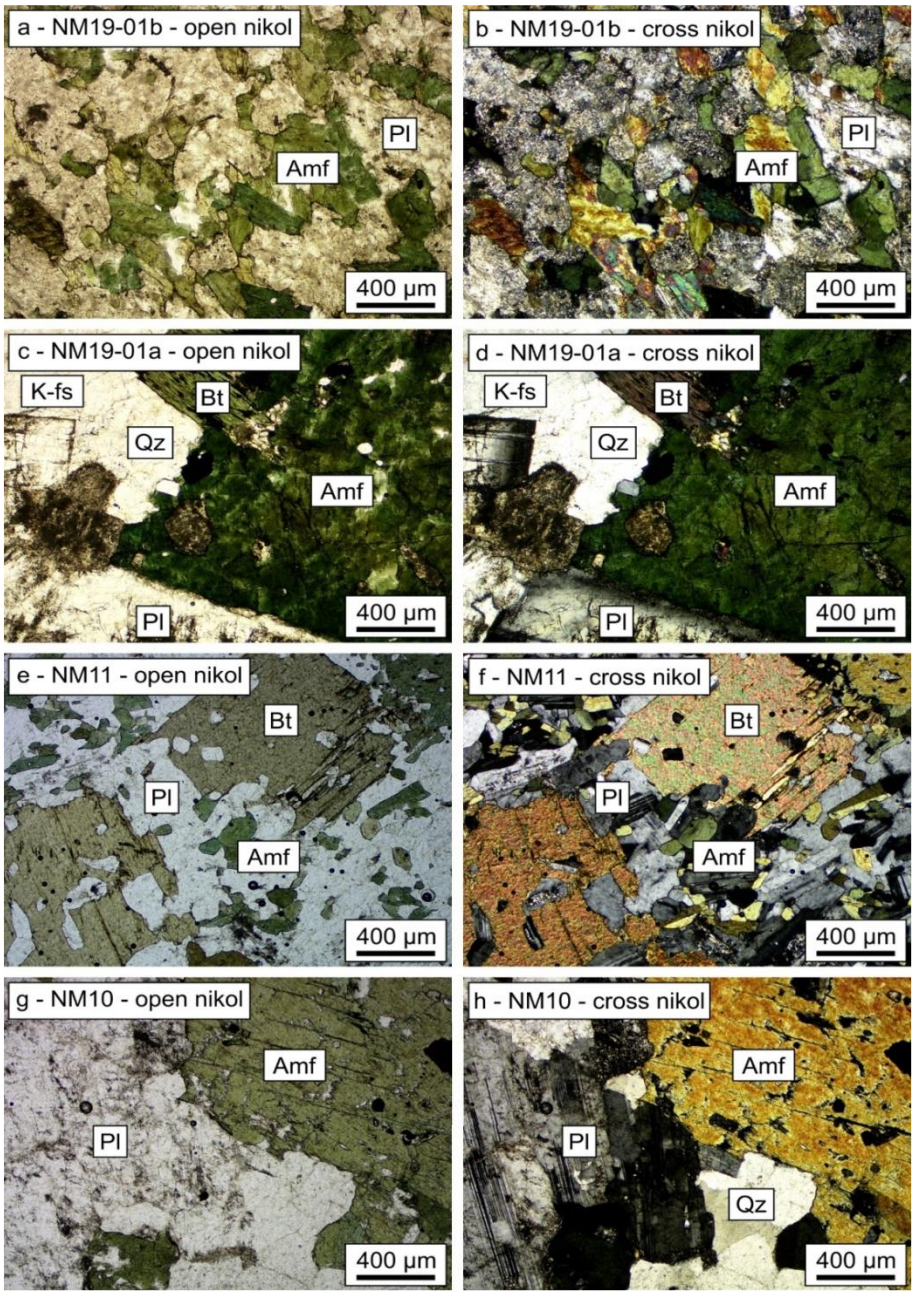

Figure 3. Photomicrograph of the Nam Meng dioritoid. a, b - low-Hf gabbro-doirite, c, d - low-Hf quartz diorite, e, f - high-Hf gabbro-diorite, g, h - high-Hf quartz diorite. Amf - amphibole, Bt - biotite, Pl - plagioclase, Qz - quartz

3.2. Geochemistry

3.2.1. Whole-rock chemistry

The SiO_2 contents of the Nam Meng gabbro-diorite and quartz diorite vary from 51.8 to 57.6 wt.% and 61.5 to 67.2 wt.% (Table 1; Fig. 4). There is one granite sample that has a high content of SiO_2 (72.6 wt.%) belonging to the high-Hf series. The total alkaline (Na_2O + K_2O) of the Nam Meng dioritoid varies from

3.72 to 5.77 wt.% with $Na_2O/K_2O > 1$. The Al_2O_3 contents of the low-Hf gabbro-diorite are lower than those of the high-Hf gabbro-diorite (14.0-17.6 wt.% and 18.0-19.4, respectively). However, the low-and high-Hf Nam Meng quartz diorite show no difference (15.2-17.2 wt.% and 15.6-16.4 wt.%, respectively). Most of Nam Meng dioritoid is metalumious. Only two samples were plotted into peraluminous (Table 1; Figs. 4, 5).

The MgO contents of the low-Hf dioritoid (5.61-6.12 wt.% and 2.16-3.49 wt.% for gabbro-diorite and quartz diorite, respectively) are higher than those of the high-Hf dioritoid (2.83-3.42 wt.% and 1.81-2.23 wt.% for gabbro-diorite and quartz diorite, respectively). In contrast, the Na_2O contents of the low-Hf dioritoid (2.58-2.99 wt.% and 2.73-3.24 wt.% for gabbro-diorite and quartz diorite, respectively) are lower than those of the high-Hf dioritoid (3.24-4.12 wt.% and 3.28-3.45 wt.% for gabbro-diorite and quartz diorite, respectively) (Table 1; Fig. 5).

Table 1. Whole-rock chemistry of the Nam Meng dioritoid

No.	1	2	3	4	5	6	7
Sample	**NM19-02**	**NM19-01B**	**NM-06**	**NM-11***	**NM-02***	**NM-04***	**H207/92**
Series	***Low-Hf gabbro diorite***			***High-Hf gabbro diorite***			
SiO_2	51.8	54.2	55.8	52.4	52.8	54.7	57.6
TiO_2	0.81	0.68	0.85	0.79	0.65	0.73	0.64
Al_2O_3	17.6	16.0	14.0	18.9	18.8	19.4	18.0
T-Fe_2O_3	9.53	8.31	10.6	9.91	10.2	8.27	7.40
MnO	0.19	0.29	0.28	0.24	0.32	0.24	0.16
MgO	5.61	6.12	5.66	3.42	3.42	2.83	3.10
CaO	9.05	8.80	5.56	7.49	7.33	7.35	6.31
Na_2O	2.99	2.88	2.58	3.98	3.51	4.12	3.24
K_2O	0.73	1.21	2.73	1.77	1.95	1.65	1.61
P_2O_5	0.21	0.10	0.22	0.16	0.13	0.16	0.14
LOI	1.30	1.32	1.57	1.06	1.25	0.92	2.34
Total	**99.8**	**99.9**	**99.9**	**100.1**	**100.4**	**100.4**	**100.5**
Rb	10.6	17.8	49.9	67.0	62.0	56.0	66.0
Cs	0.35	0.26	0.38	1.40	2.20	2.10	
Sr	294	252	167	285	268	317	306
Ba	171	209	474	323	387	368	289
Sc	14.7	15.8	22.8	17.0	22.0	14.0	7.00
Zr	145	84.0	229	113	73.0	89.0	101
Hf	0.68	0.91	1.02	3.00	2.60	2.80	8.08
Nb	4.46	6.67	9.86	5.00	8.00	9.00	6.90
Ta	0.28	0.51	0.79	0.40	0.80	0.70	0.46
Y	24.0	23.8	50.6	27.0	43.0	30.0	34.0
La	10.4	9.60	17.4	14.8	12.5	17.1	11.7
Ce	26.3	29.9	46.5	36.1	32.7	44.2	36.8
Pr	3.46	4.07	6.55	4.91	5.23	6.35	
Nd	15.4	17.1	28.3	21.0	25.7	28.0	25.1
Sm	3.96	3.95	7.32	5.20	7.50	6.70	5.63
Eu	1.00	1.04	1.24	1.41	1.57	1.59	1.36
Gd	3.81	3.60	6.87	5.00	7.40	6.10	
Tb	0.64	0.59	1.17	0.80	1.30	1.00	1.21
Dy	3.92	3.66	7.43	5.60	8.20	6.40	
Ho	0.73	0.70	1.41	1.10	1.60	1.20	
Er	2.29	2.29	4.58	3.40	5.10	3.90	
Tm	0.35	0.37	0.73	0.50	0.78	0.60	
Yb	2.18	2.48	4.80	3.50	5.70	4.40	4.99

Lu	0.32	0.40	0.75	0.54	0.90	0.68	0.66
V	135	169	112	185	118	91.0	121
Cr	37.0	45.0	40.0		20.0		19.0
Co	22.2	21.5	21.9	19.0	15.0	14.0	19.0
Ni	6.34	9.62	12.0		20.0		6.00
Cu	27.4	11.8	34.0	60.0	10.0		16.0
Zn	70.0	80.0	121	90.0	110	90.0	68.0
Pb	3.02	6.08	4.36		6.00	6.00	5.00
Mo	0.41	0.06	0.13				
Sn	1.13	1.94	3.04	1.00	2.00	2.00	
W	0.20	0.15	0.25				
Th	1.90	1.53	6.98	2.60	3.40	5.00	3.40
U	0.49	0.65	1.77	0.70	1.80	1.30	

Table 1. (cont.)

No.	8	9	10	11	12	13
Sample	**NM19-03**	**NM19-01A**	**NM-07**	**NM19-08**	**NM19-05**	**NM19-07**
Series	***Low-Hf quartz diorite***					
SiO_2	61.5	61.6	62.9	63.1	66.1	67.2
TiO_2	0.58	0.60	0.47	0.48	0.38	0.34
Al_2O_3	17.2	15.8	16.3	16.0	15.2	15.3
T-Fe_2O_3	5.58	6.02	5.23	5.64	4.68	3.84
MnO	0.15	0.15	0.12	0.14	0.12	0.09
MgO	2.78	3.49	3.13	3.11	2.40	2.16
CaO	6.59	5.12	3.92	5.65	5.08	5.12
Na_2O	3.13	2.73	3.24	2.89	2.97	2.88
K_2O	1.18	2.12	2.46	1.82	1.95	2.14
P_2O_5	0.19	0.15	0.14	0.13	0.14	0.12
LOI	0.97	1.97	1.98	1.03	0.80	0.73
Total	**99.8**	**99.8**	**99.9**	**99.9**	**99.8**	**99.9**
Rb	16.3	40.9	44.0	35.6	68.7	34.4
Cs	0.62	0.74	0.48	1.21	0.70	1.13
Sr	321	214	154	193	194	180
Ba	443	472	405	329	308	431
Sc	5.59	8.28	7.24	8.02	8.52	5.82
Zr	140	133	142	130	157	105
Hf	0.38	0.47	0.58	0.74	0.61	0.64
Nb	7.27	6.94	5.44	5.39	5.06	4.18
Ta	0.57	0.63	0.54	0.55	0.49	0.58
Y	13.5	15.5	13.7	14.8	19.2	10.4
La	15.4	13.1	5.61	15.2	20.5	25.5
Ce	40.2	29.9	18.0	33.2	42.8	51.8
Pr	4.09	3.44	1.89	3.48	4.50	4.35
Nd	15.1	12.7	7.9	12.4	15.8	13.3
Sm	2.97	2.66	2.00	2.48	3.17	2.11
Eu	0.95	0.76	0.62	0.70	0.76	0.63
Gd	2.70	2.51	1.92	2.38	3.03	2.10
Tb	0.39	0.40	0.33	0.37	0.47	0.28
Dy	2.22	2.43	2.12	2.23	2.89	1.59
Ho	0.40	0.46	0.41	0.43	0.55	0.30
Er	1.28	1.51	1.35	1.40	1.80	0.98
Tm	0.20	0.24	0.22	0.22	0.29	0.16
Yb	1.34	1.64	1.52	1.54	1.98	1.14
Lu	0.21	0.26	0.25	0.24	0.32	0.19
V	18.0	83.7	68.0	85.0	84.0	80.0

Cr	49.0	98.4	30.0	23.0	18.0	24.0
Co	8.09	12.5	10.2	11.0	15.0	20.0
Ni	4.31	3.43	3.01	2.81	2.78	2.26
Cu	4.32	5.39	18.0	4.10	6.40	3.46
Zn	64.6	61.6	65.0	49.7	41.0	34.7
Pb	7.49	6.55	3.75	6.13	6.63	8.10
Mo	0.06	0.21	0.09	0.21	0.27	0.08
Sn	1.01	1.42	1.37	1.35	1.48	0.96
W	0.14	0.16	0.41	0.27	0.35	0.23
Th	3.16	6.20	3.62	8.85	12.1	17.9
U	0.46	1.28	1.49	1.89	1.84	2.20

Table 1. (cont.)

No.	14	15	16	17	18	19
Sample	**H229/92**	**NM-05***	**H213/92**	**NM-10***	**H233/92**	**H227/92**
Series	***High-Hf quartz diorite***					
SiO_2	63.1	63.6	64.3	64.4	72.6	65.2
TiO_2	0.48	0.44	0.42	0.47	0.28	0.44
Al_2O_3	15.8	16.3	16.4	16.0	13.5	15.6
T-Fe_2O_3	5.76	5.52	5.28	5.39	2.41	5.10
MnO	0.15	0.13	0.13	0.12	0.03	0.13
MgO	2.23	1.87	1.87	1.92	0.49	1.81
CaO	5.37	5.44	5.26	5.19	1.07	4.91
Na_2O	3.28	3.44	3.28	3.31	2.69	3.45
K_2O	2.36	1.49	1.91	1.94	5.32	1.71
P_2O_5	0.20	0.13	0.09	0.12	0.05	0.12
LOI	1.41	1.22	1.29	0.77	1.26	1.86
Total	**100.1**	**99.6**	**100.3**	**99.6**	**99.7**	**100.4**
Rb	68.5	53.0	70.0	70.0	156	64.4
Cs		1.20		1.60		
Sr	216	273	237	251	146	220
Ba	467	337	354	399	760	330
Sc	12.0	7.00	10.0	8.00	8.00	11.0
Zr	151	146	88.0	117	158	121
Hf	5.03	3.70	6.03	3.10	5.95	4.69
Nb	7.90	5.00	6.90	5.00	13.80	8.00
Ta	0.85	0.40	0.67	0.50	1.00	1.21
Y	23.4	15.0	15.6	16.0	25.0	17.6
La	20.0	22.4	27.2	12.8	47.4	32.5
Ce	40.6	39.2	44.3	26.4	75.7	55.2
Pr	4.76	4.16		3.25		5.80
Nd	19.1	14.5	34.3	12.8	31.8	20.4
Sm	3.88	3.10	3.21	2.90	6.28	3.34
Eu	0.90	0.91	0.86	0.87	0.92	0.71
Gd	3.92	2.80		2.80		3.25
Tb	0.68	0.50	0.71	0.50	1.08	0.53
Dy	3.76	3.00		3.00		2.98
Ho	0.88	0.60		0.60		0.65
Er	2.44	1.90		1.90		1.81
Tm	0.37	0.28		0.29		0.37
Yb	2.67	1.90	2.54	2.10	2.41	2.06
Lu	0.45	0.31	0.40	0.33	0.43	0.36
V	93.0	65.0	76.0	73.0	16.0	81.0
Cr	13.0		12.0		14.0	8.0
Co	9.00	10.0	14.0	10.0	2.30	7.00

Ni	2.00		4.00		3.00	1.00
Cu	5.00		4.00		5.00	4.00
Zn	70.0	60.0	67.0	60.0	41.0	85.0
Pb	11.0		8.00		23.0	11.0
Mo						
Sn		1.00		1.00		
W						
Th	14.6	8.00	10.9	7.30	23.0	20.6
U	2.60	1.50	1.50	1.80	2.90	2.00

* From Tran et al. (2022)

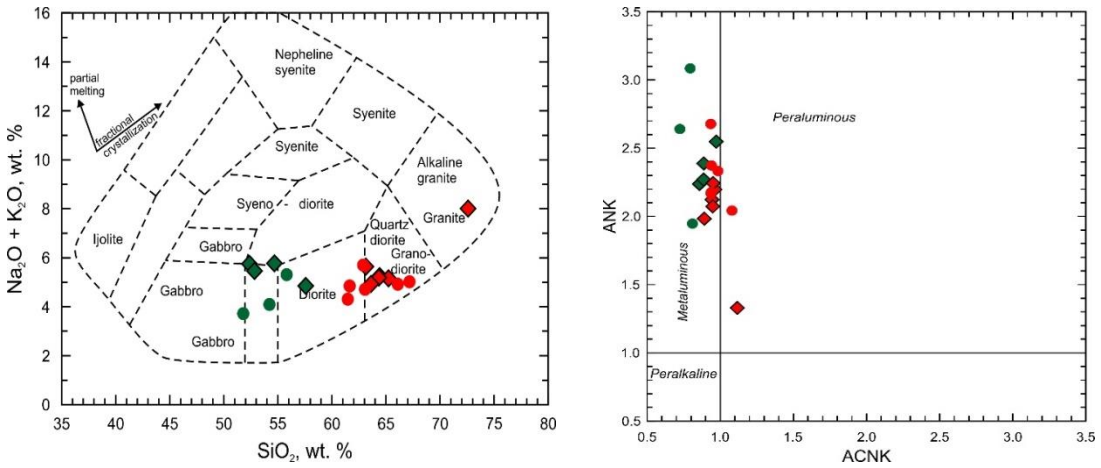

Figure 4. TAS (left) and ACNK-ANK (right) classification diagrams of the Nam Meng dioritoid. The TAS diagram for plutonic rocks is adapted from Cox et al. (1979) by Wilson (1989). ACNK = $Al_2O_{3molar}/(CaO+Na_2O+K_2O)_{molar}$, ANK = $Al_2O_{3molar}/(Na_2O+K_2O)_{molar}$. See Fig. 1 for symbols legend

The TiO_2, T-Fe_2O_3, and CaO contents of the gabbro-diorite (0.64-0.85 wt.%, 7.4-10.6 wt.%, and 5.56-9.05 wt.%, respectively) are higher than those of the quartz diorite (0.34-0.60 wt.%, 3.84-6.02 wt.%, and 3.92-6.59 wt.%, respectively) (Table 1; Fig. 5). There is no significant difference between low- and high-Hf series at the TiO_2, T-Fe_2O_3, and CaO contents.

The K_2O and P_2O_5 contents are similar for low- and high-Hf diorite (Table 1; Fig. 5). Most samples belong to the low-K calc-alkaline series. Only 3 samples belong to the high-K calc-alkaline series (Fig. 5). Despite K_2O and P_2O_5, other major oxide contents negatively correlate with the SiO_2 contents. The granite sample has the highest content of SiO_2 and K_2O and the lowest content of other major oxides (Table 1; Fig. 5).

The low-Hf gabbro-diorite's large ion lithophile elements (LILE - Ba and Sr) and high field strength elements (HSFE - Zr, Nb) of vary widely. They cover most of the data of the high-Hf dioritoid and high-Hf quartz diorite (Ba = 171-474 ppm, Sr = 167-294 ppm, Zr = 84.0-229 ppm, and Nb = 4.46-9.86 ppm). The Ba and Nb contents of the high-Hf quartz diorite (289-387 and 6.90-9.00 ppm, respectively) are similar to those of the high-Hf dioritoid (308-472 and 4.18-8.00 ppm, respectively). Rb contents of the high-Hf gabbro-diorite (56.0-67.0 ppm) are similar to those of the high-Hf quartz diorite (53.0-70.0), and both of them are higher than the low-Hf gabbro-diorite (Rb = 10.6-49.9 ppm) and low-Hf quartz diorite (16.3-44.0 ppm).

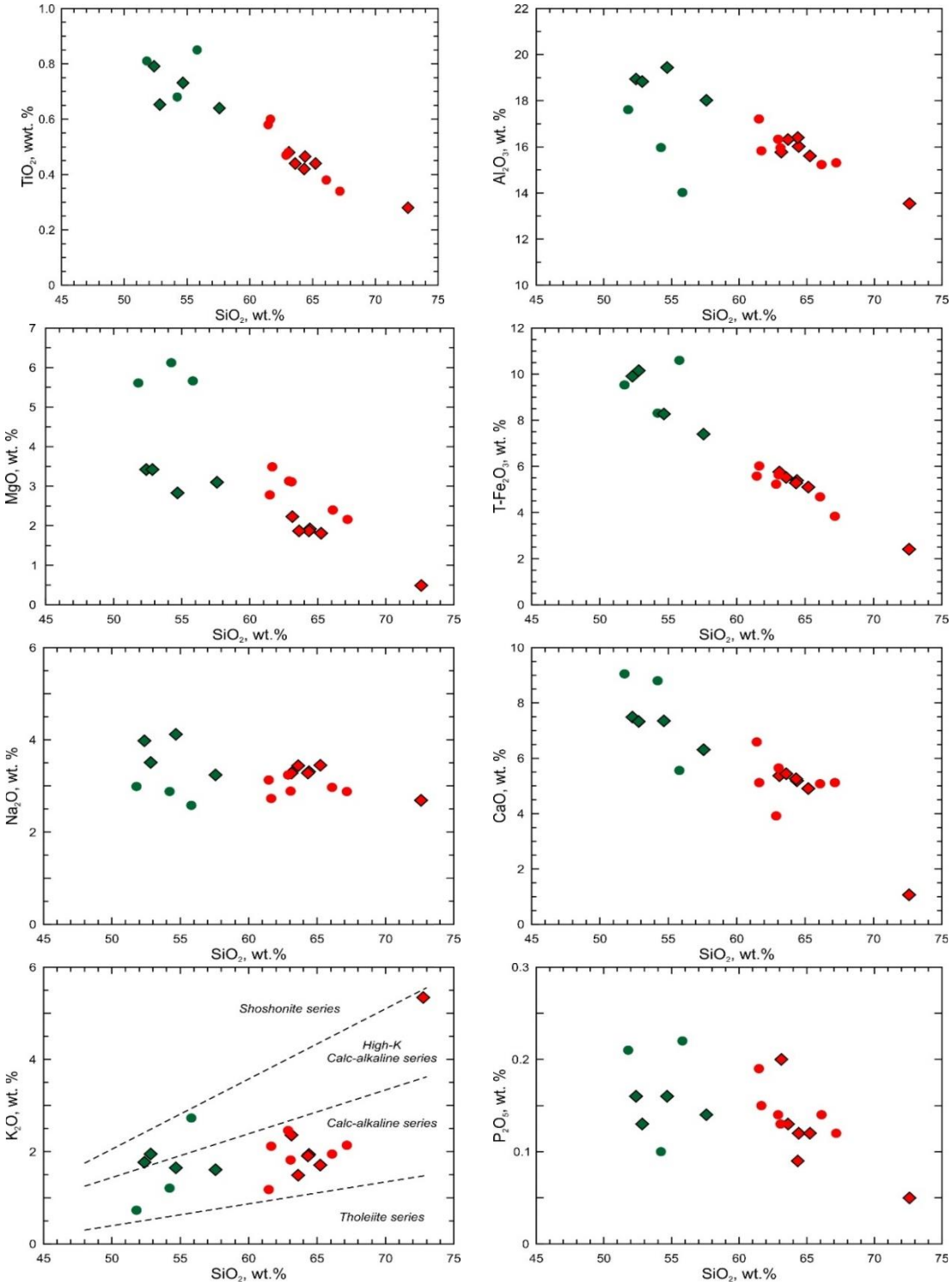

Figure 5. Harker diagrams (Harker, 1909) of major oxides vs SiO_2 of the Nam Meng dioritoid. Field in the SiO_2 vs K_2O diagram after Rickwood (1989) and Le Maitre et al. (1989)

The Zr contents of the high-Hf dioritoid (73.0-113 ppm) are lower than those of the quartz diorite (88.0-157 ppm) while the Sr contents of the high-Hf dioritoid (268-317 ppm) are higher than those of the quartz diorite (216-287 ppm). The sample NM19-03 of the low-Hf quartz diorite has a significantly high concentration of Sr (471 ppm) (Table 1; Fig. 6).

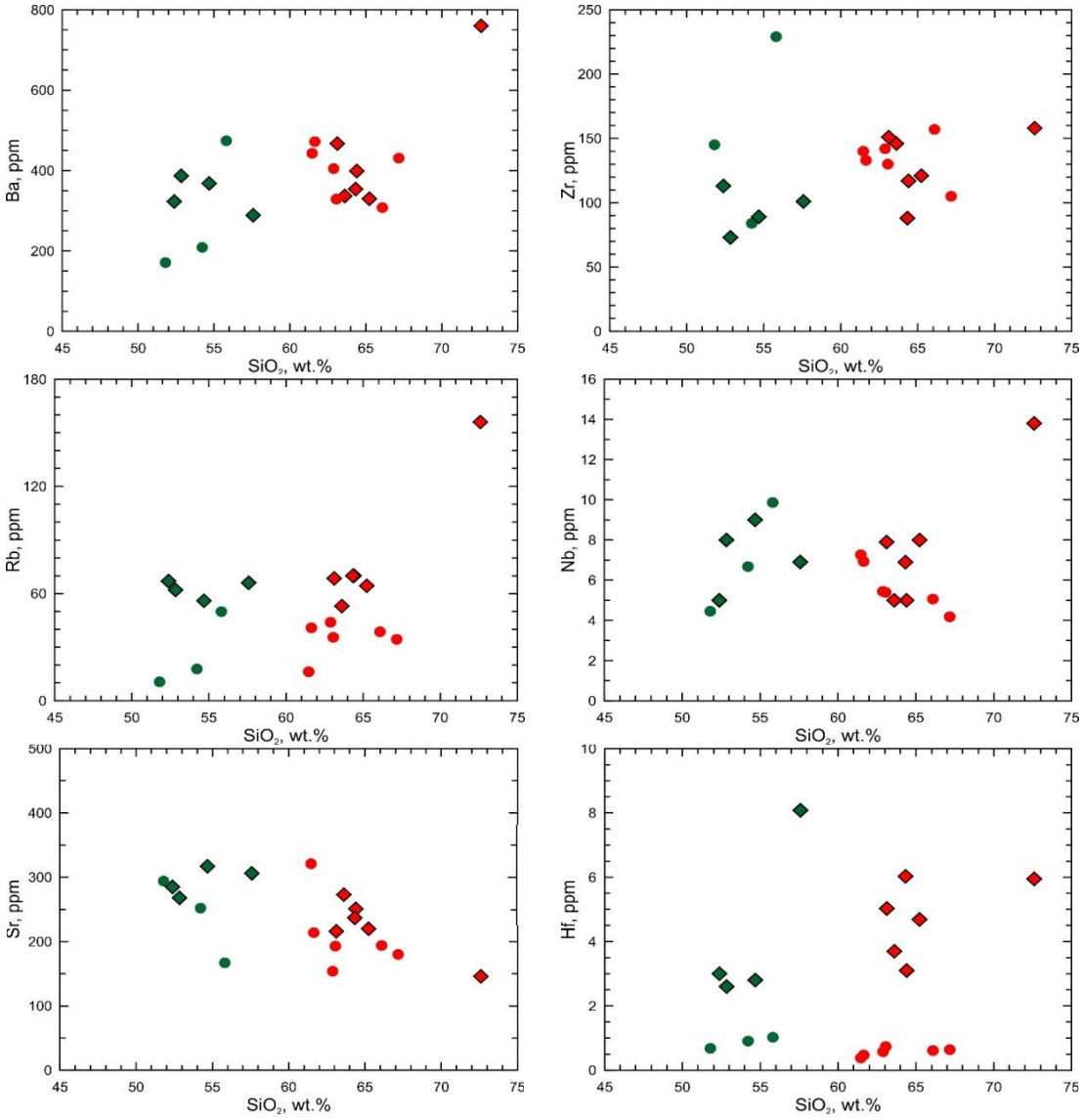

Figure 6. Harker diagram (Harker, 1909) of the LILE and HFSE vs SiO_2 of the Nam Meng dioritoid

The gabbro-diorite's light rare earth elements (LREE) are lower than the quartz diorite. In contrast, the gabbro diorite's heavy rare earth elements (HREE) are higher than the quartz diorite's. Among the gabbro-diorite, the LREE are slightly enriched compared with the HREE (La/Yb = 1.5-3.2), while among the quartz diorite, the LREE are highly enriched compared with the HREE (La/Yb = 4.1-15.1) (Fig. 7). Most of samples have weakly negative anomaly of Eu (Eu/Eu* = 0.53- 0.97) except the sample NM19-03 has weakly

positive anomaly of Eu (Eu/Eu* = 1.02). The HREE of the high-Hf series is relatively higher than those of the low-Hf series. There is no difference in the LREE of the low- and high-Hf dioritoid.

The Hf shows a tendency difference from other HSFE. The Hf contents of the low-Hf gabbro-diorite and quartz diorite vary in a small range (0.68-1.02 and 0.38-0.74 ppm). Most of the Hf contents of the high-Hf gabbro-diorite vary from 2.60 to 3.00 ppm. The sample H207/92 of the hight-Hf gabbro-diorite has a significantly high concentration of Hf (8.08 ppm). The Hf contents of the high-Hf quartz diorite vary from 3.10 to 6.03 ppm (Table 1; Fig. 6).

3.2.2. Sr and Nd isotopic ratios

The $^{87}Sr/^{86}Sr$ of the low-Hf gabbro-diorite and low-Hf quartz diorite vary in a broader range (0.70519-0.71108, 0.70649-0.70948, respectively) than of the high-Hf gabbro-diorite and high-Hf quartz diorite (0.70729-0.70824 and 0.70702-0.70862, respectively). The ε_{Nd} of the low-Hf quartz diorite (-4.12 to -1.66) vary in a broader range than the low-Hf gabbro-diorite, high-Hf gabbro-diorite and high-Hf quartz diorite (-2.56 to -0.55, -3.10 to -0.70, and -4.47 to -1.24) (Table 2). The Nam Meng dioritoid have negative ε_{Nd} and most of them are shifted away from the mantle array to the right side.

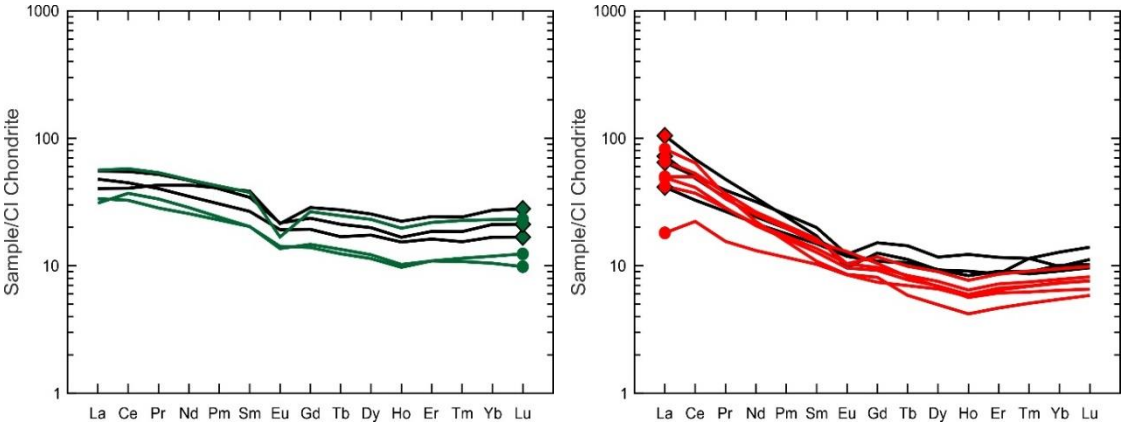

Figure 7. REE chondrite normalized patterns of the Nam Meng dioritoid. The chondrite was valued after Boynton (1984)

Table 2. Sr and Nd isotopic ratios of the Nam Meng dioritoid

Sample	**NM19-02**	**NM19-01b**	**NM-06**	**NM-11**	**NM-02**	**NM-04**	**H207/92**
Series	***Low-Hf gabbro-diorite***			***High-Hf gabbro-diorite***			
$^{87}Rb/^{86}Sr$	0,101	0,197	0,834	0,656	0,646	0,493	0,602
$^{87}Sr/^{86}Sr$	0,70519	0,70697	0,71108	0,70729	0,70824	0,70739	0,70778
$^{87}Sr/^{86}Sr_{290\ Ma}$	0,70477	0,70616	0,70764	0,70458	0,70557	0,70535	0,70530
$^{147}Sm/^{144}Nd$	0,1586	0,1422	0,1594	0,1526	0,1799	0,1475	0,1383
$^{143}Nd/^{144}Nd$	0,512610	0,512507	0,512602	0,512596	0,512517	0,512479	0,512602
$^{143}Nd/^{144}Nd_{290\ Ma}$	0,512309	0,512237	0,512299	0,512306	0,512176	0,512199	0,512339
T_{DM2} (Ma)	1,49	1,37	1,54	1,38	2,83	1,54	1,11
ε_{Nd}	-0,55	-2,56	-0,70	-0,82	-2,36	-3,10	-0,70
$\varepsilon_{Nd\ 290\ Ma}$	0,86	-0,54	0,68	0,81	-1,74	-1,28	1,46

Note: $(^{143}Nd/^{144}Nd)_{CHUR,\ today}$ = 0.512638 (Goldstein et al., 1984); $(^{143}Nd/^{144}Nd)_{DM,\ today}$ = 0.51315, $(^{147}Sm/^{144}Nd)_{DM,\ today}$ = 0.2137 (Peucat et al., 1988)

Table 2 (cont.)

Sample	NM19-03	NM19-01a	NM-07	NM19-08	NM19-05	NM19-07
Series	*Low-Hf quartz diorite*					
$^{87}Rb/^{86}Sr$	0,142	0,534	0,798	0,515	0,557	0,533
$^{87}Sr/^{86}Sr$	0,70649		0,70948	0,70813	0,70761	0,70833
$^{87}Sr/^{86}Sr_{290\ Ma}$	0,70590		0,70619	0,70600	0,70531	0,70613
$^{147}Sm/^{144}Nd$	0,1214	0,1285	0,1561	0,1237	0,1233	0,0976
$^{143}Nd/^{144}Nd$	0,512447	0,512465	0,512574	0,512494	0,512548	0,512409
$^{143}Nd/^{144}Nd_{290\ Ma}$	0,512217	0,512221	0,512278	0,512259	0,512314	0,512224
T_{DM2}	1,16	1,22	1,52	1,11	1,02	0,97
ε_{Nd}	-3,72	-3,37	-1,24	-2,81	-1,76	-4,47
$\varepsilon_{Nd\ 290\ Ma}$	-0,93	-0,85	0,26	-0,11	0,96	-0,80

Table 2 (cont.)

Sample	H229/92	NM-05	H213/92	NM-10	H227/92	H233/92
Series	*High-Hf quartz diorite*					
$^{87}Rb/^{86}Sr$	0,885	0,542	0,824	0,778	0,817	2,983
$^{87}Sr/^{86}Sr$	0,70862	0,70702	0,70850	0,70767	0,70855	0,72682
$^{87}Sr/^{86}Sr_{290\ Ma}$	0,70497	0,70478	0,70510	0,70446	0,70518	0,71451
$^{147}Sm/^{144}Nd$	0,1255	0,1318	0,0577	0,1396	0,1009	0,1217
$^{143}Nd/^{144}Nd$	0,512511	0,512510	0,512427	0,512553	0,512446	0,512272
$^{143}Nd/^{144}Nd_{290\ Ma}$	0,512273	0,512260	0,512317	0,512288	0,512254	0,512041
T_{DM2}	1,10	1,19	0,71	1,23	0,95	1,45
ε_{Nd}	-2,48	-2,49	-4,12	-1,66	-3,75	-7,14
$\varepsilon_{Nd\ 290\ Ma}$	0,16	-0,09	1,03	0,46	-0,20	-4,37

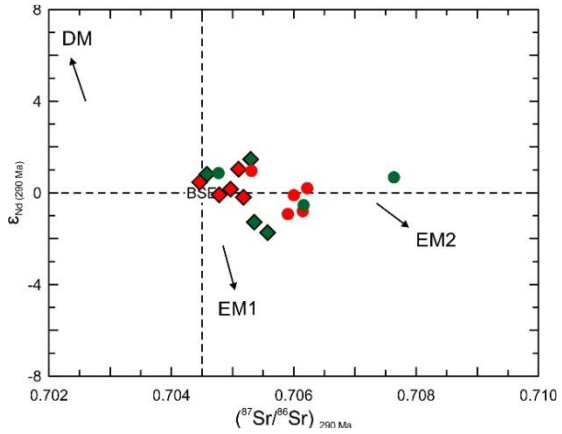

Figure 8. $^{87}Sr/^{86}Sr$ vs ε_{Nd} diagram for the Nam Meng dioritoid at present (left) and at 290 Ma (right)

4. Discussions

4.1. Tectonic setting

Early studies on the whole-rock geochemistry (calc-alkaline series) and Ar-Ar biotite age (250 ± 15 Ma) of the Dien Bien complex suggested that the rocks were formed at the collision stage of the convergence margin (Izokh, 1971; Tran, 1994). Recent studies about the U-Pb zircon age (290-280 Ma) and trace elements of the Nam Meng and Nam Po suggested that their rock was formed at the subduction stage of the amalgamation of the Indochina and Sino-Vietnam composite terrane (Liu et al., 2012; Hieu, 2017; Hieu et al., 2017; Tran et al.,

2022). The results of this study support the latter.

The mineral assemblages of the Nam Meng dioritoid comprise significant amounts of plagioclase, amphibole, lesser amounts of biotite and quartz, and small amounts of K-feldspar (Fig. 3). Muscovite is not observed. The ACNK and ANK indexes of the Nam Meng dioritoid are mostly metaluminous. All the ACNK are less than 1.1 (Fig. 4). The PM normalized patterns of the trace elements of the Nam Meng dioritoid show negative anomalies of the Ta, Nb, and Ti (Fig. 9). These mineralogical and geochemical characteristics and the Y-Nb and Y+Nb-Rb discrimination diagrams (Fig. 10) suggest that the Nam Meng dioritoid is an I-type granitic rock (Chappell and White, 1974) and was formed in a subduction environment.

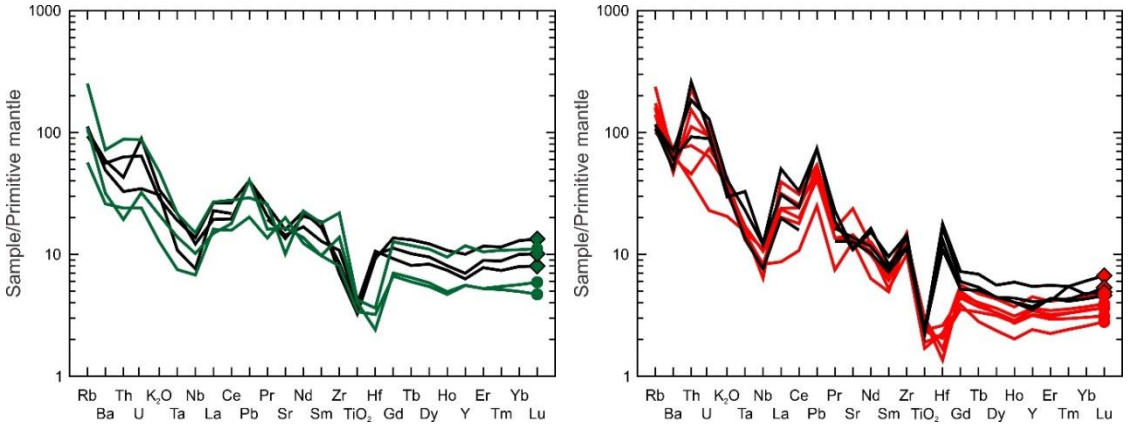

Figure 9. Spider diagrams of the Nam Meng dioritoid.
Primitive mantle values after McDonough and Sun (1995)

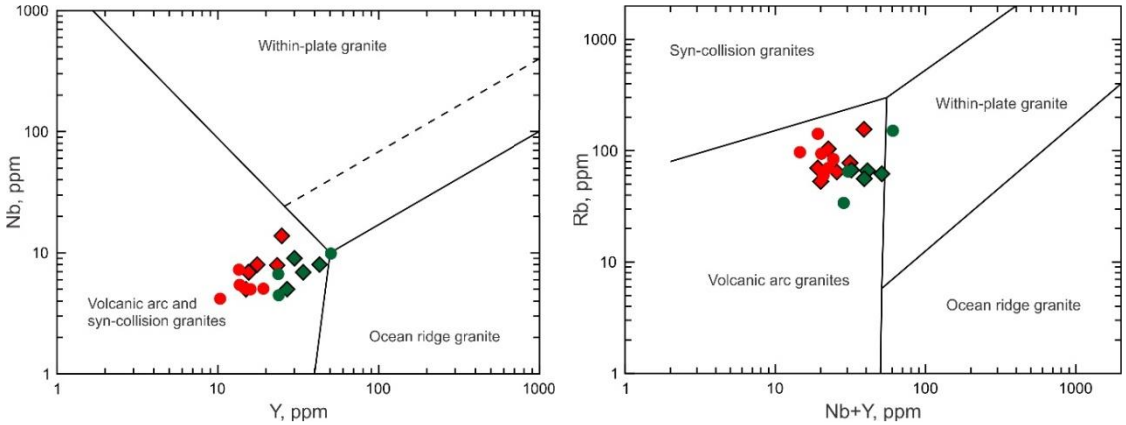

Figure 10. The Y-Nb (left) and Y+Nb-Rb (right) discrimination diagrams for the Nam Meng dioritoid (Pearce et al., 1984)

4.2. Magmatic differentiation

Petrography of the Nam Meng intrusion varies from gabbro-diorite to quartz diorite, granodiorite, and granite (Izokh, 1971; Tran, 1994). Among the Nam Meng gabbro-diorite and quartz diorite, there is a negative

correlation between SiO_2 and Al_2O_3, MgO, T-Fe_2O_3, and CaO (Fig. 5). Although the low-Hf dioritoid has higher MgO contents than those of the high-Hf dioritoid, they maintain the negative anomaly inside each series (Fig. 5). The high concentrations of the MgO caused the low concentrations of the Al_2O_3 in the low-Hf gabbro-diorite. The Al_2O_3 + MgO shows an excellent negative correlation with the SiO_2 (Fig. 11).

During the magmatic differentiation, Ti prefers to stay in the melt. Therefore, the SiO_2 and TiO_2 correlation should be positive. The negative correlation between the SiO_2 and TiO_2 of the Nam Meng dioritoid is quite strange (Fig. 5). However, the presence of biotite in the gabbro-diorite and biotite in the quartz diorite could explain this. The early crystallization of the biotite traps the Ti from the melt causing this phenomenon.

The total alkaline, Na_2O, and K_2O show no correlation with the SiO_2. On the other hand, the total alkaline has a strongly positive correlation with the Hf in the low-Hf series and a weakly negative correlation with the Hf in the high-Hf series (Fig. 12).

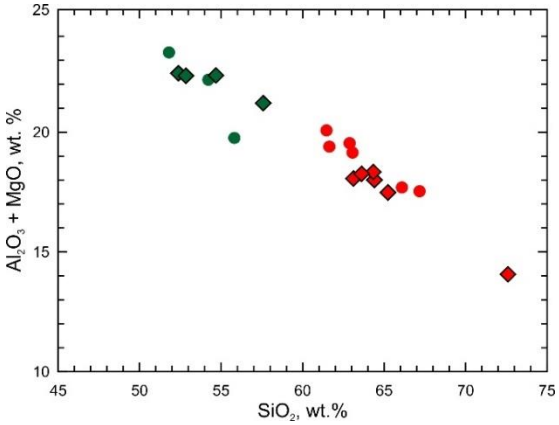

Figure 11. SiO_2 vs Al_2O_3 + MgO diagram for the Nam Meng dioritoid

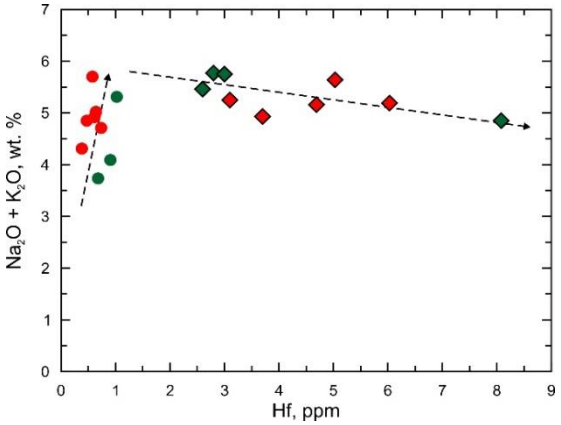

Figure 12. Hf vs Na_2O + K_2O diagram for the Nam Meng dioritoid

Therefore, serial petrography and correlation among the major oxides suggest that the concentration of the Nam Meng dioritoid was caused by the magmatic differentiation process. The concentration of the total alkaline in the Nam Meng dioritoid could not be explained by the magmatic differentiation but by another process discussed in the following section.

4.3. Magma origin

4.3.1. Possibility of the continental crust contamination

Before discussing the source of the mantle that was melted to form the Nam Meng magma, we would like to consider the possibility of continental crust contamination. The continental crust is rich in LILE (Ba, Rb, and Sr) and low HSFE (Zr, Nb, and Ta) (Rudnick and Fountain, 1995; Rudnick and Gao, 2003; Hu and Gao, 2008). The contamination of the continental crust causes an increase of the Ba, $^{87}Sr/^{86}Sr$ compared with the Nb and Zr. In other words, the Ba/Nb and $^{87}Sr/^{86}Sr$ ratios would positively correlate. The Ba/Nb and $^{87}Sr/^{86}Sr$ ratios of the Nam Meng dioritoid have no positive correlation. Particularly, Ba/Nb and $^{87}Sr/^{86}Sr$ have a negative correlation in low-Hf series and high-Hf quartz diorite (Fig. 13). Hoang and Uto (2003) proposed a mantle array for the Ti/Zr vs Ba/Zr diagram. Most of the Nam

Neng dioritoid (except sample NM-02) is plotted below the mantle array. Therefore, the Nam Meng magma had not been contaminated by the continental crust and maintained the geochemical characteristics of the original melt.

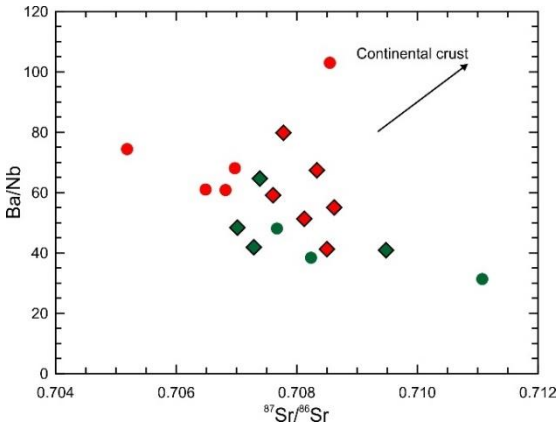

Figure 13. $^{87}Sr/^{86}Sr$ vs Ba/Nb diagram for the Nam Meng dioritoid

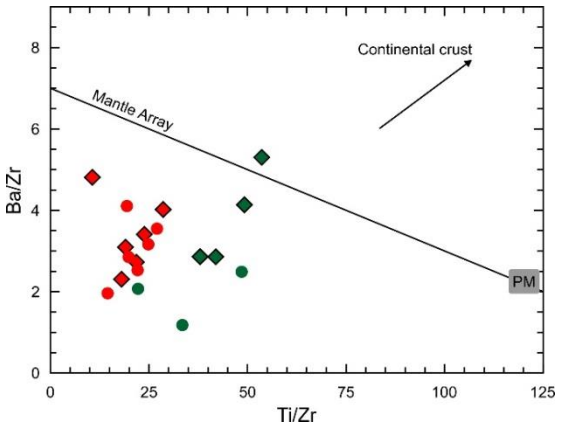

Figure 14. Ti/Zr vs Ba/Zr diagram for the Nam Meng dioritoid. Primitive mantle (PM) after McDonough and Sun (1995), Mantle Array after Hoang and Uto (2003)

4.3.2. Mantle origin

The composition of the mantle that was melted to form magma could be determined by the La/Yb ratios. Using the theoretical melting model by McKenzie and Bickle (1988), Johnson et al. (1990), and McKenzie and O'Nions (1991), Hoang (2023) reported that melting a spinel peridotite results in low La/Yb ratio (less than 15) and melting from a garnet peridotite results in a high La/Yb ratio (greater than 20). A spinel-garnet peridotite results in an intermediate La/Yb ratio (15-20). The less differentiated Nam Meng gabbro-diorite has low La/Yb ratios (1.48-3.21; Table 1; Fig. 15). It suggests that the Nam Meng dioritoid was derived from a magma that melted from a spinel peridotite mantle.

The $\varepsilon_{Nd\ (290\ Ma)}$ of the Nam Meng dioritoid are close to bulk earth silicate at 290 Ma (BSE; -1.74 to 1.46; Table 2). The $^{87}Sr/^{86}Sr_{(290\ Ma)}$ of the Nam Meng dioritoid varies in a wide range from intermediate to high (0.70446 to 0.70764; Table 2). The Sr and Nd isotope of the Nam Meng dioritoid is plotted among the depleted mantle (DM), enriched mantle 1 (EM1), and enriched mantle 2 (EM2) (Fig. 8; after Hofmann and White, 1982; White and Hofmann, 1982; Zindler and Hart, 1986) suggesting that the Nam Meng magma resulted from mixing among DM, EM1, and EM2 sources.

Hieu et al. (2017) proposed that the Nam Meng granodiorite was derived from remelting of oceanic basalt source based on the low concentrations of MgO, Cr, and Ni and the similar between Nb/Ta and Zr/Hf (15.9 ± 0.6 and 35.5-45.5, respectively) ratios with those of oceanic island basalt (OIB). The low concentration of MgO, Cr, and Ni in the granodiorite could be explained by the magmatic differentiation (Fig. 5). The Nb/Ta and Zr/Hf ratios of the Nam Meng granodiorite are in the wide range of the Nam Meng dioritoid (Table 1). On the other hand, the Nam Meng dioritoid has a positive anomaly of Pb (Fig. 9). Therefore, the oceanic crust is considered a member involved in

forming the Nam Meng spinel peridotite mantle source.

The oceanic crust mixes with EM1 and EM2 in the subduction zone (Hofmann and White, 1982; White and Hofmann, 1982). That means there was ancient subduction that happened before the Indosinian event. The calculated T_{DM2} of the Nam Meng dioritoid varies in a wide range from 710 to 2,830 Ma. with mean = 1,258 ± 47 Ma (Fig. 16). It corresponds to the Meso-Neopreoterozoic Rodinia supercycle. This age is higher than the Hf model age in zircon reported by Hieu et al. (2017) for the Nam Meng granodiorite (686-670 Ma) but close to the Nam Rom granodiorite (1,184 Ma) Chieng Khuong quartz diorite (1,328 Ma) and Phia Bioc biotite granite (1,227 Ma).

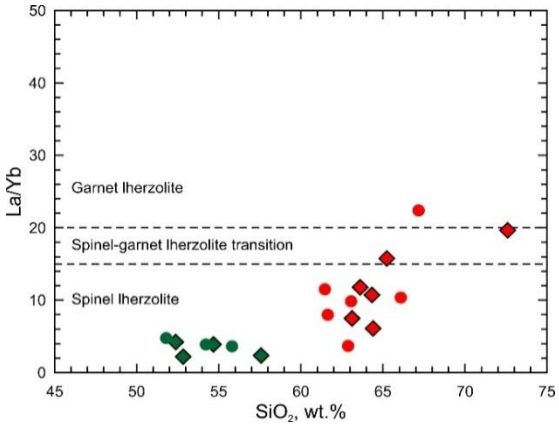

Figure 15. SiO_2 vs La/Yb diagram for the Nam Meng dioritoid. Phase boundary after Hoang (2023)

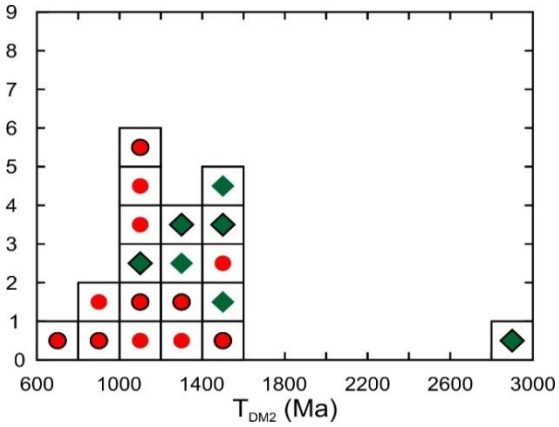

Figure 16. Histogram of Nd model age of the Nam Meng dioritoid

4.3.3. Degree of partial melting

Although the magmatic differentiation and mantle mixing processes could explain most of the major oxides geochemistry and dispersive Sr and Nd isotope of the Nam Meng dioritoid, respectively, they could not work well for the LILE and HSFE, especially Hf. In the Nam Meng massif, the less differentiated gabbro-diorite and the more differentiated quartz diorite occur together (Fig. 1). Each rock type has a low-Hf and a high-Hf series. The low-Hf Nam Meng dioritoid has a Hf negative anomaly, while the high-Hf Nam Meng quartz diorite has a Hf positive anomaly. There is no Hf anomaly in most of the high-Hf Nam Meng gabbro-diorite samples, except for the sample H207/92, which has the highest Hf content (Table 1; Figs. 6, 9).

In the subduction zone, water is released from hydrous minerals in the subducted slab and rises to the overriding mantle wedge. The water lowers the mantle wedge's melting temperature, causing partial melting to form magma. The degree of partial melting strongly affects trace elements' concentration in magma (Kimura and Yoshida, 2006; Kelly et al., 2010; Jamali, 2017). Jamali (2017) reported that, in the subduction zone, the increase in crust thickness with arc maturity caused low partial melting and more differentiation, leaving magmas with low Zr, Hf, and HREEs behind.

The difference in the Hf contents of the Nam Meng dioritoid could have resulted from the different degrees of partial melting in the subduction zone. Whereas a high degree of partial melting generated high-Hf magma, a

low degree generated low-Hf magma. Much of Hf went to the melt at a high degree of partial melting, causing low ratios of Zr/Hf and Ba/Hf. With the decrease of partial melting, less Hf went to the melt, causing the increase in the Zr/Hf and Ba/Hf ratios (Figs. 17, 18). The Zr/Hf and Ba/Hf ratios increase slowly at the high-Hf series at 2.5 to 8 ppm concentrations. Then, these ratios increase quickly at the low-Hf series at concentrations less than 1 ppm. That means the fractionation between Hf and other elements is more significant at low degree partial melting than at high partial melting. At the high degree of partial melting, the proportion of Hf that went to the melt is competitive with other LILE and HSFE elements. The Zr/Hf ratios in the melt at the high degree of partial melting are even lower than Zr/Hf in the primitive mantle ($Zr_N/Hf_N < 1$; Fig. 19). The Hf_N and Zr_N/Hf_N have a liner correlation in logarithmic scale (Fig. 19).

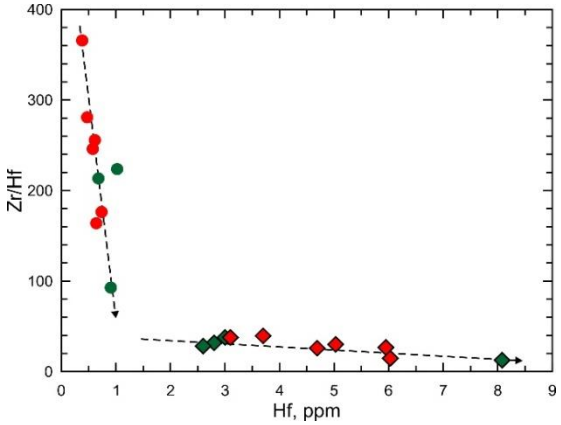

Figure 17. Hf vs Zr/Hf diagram for the Nam Meng dioritoid

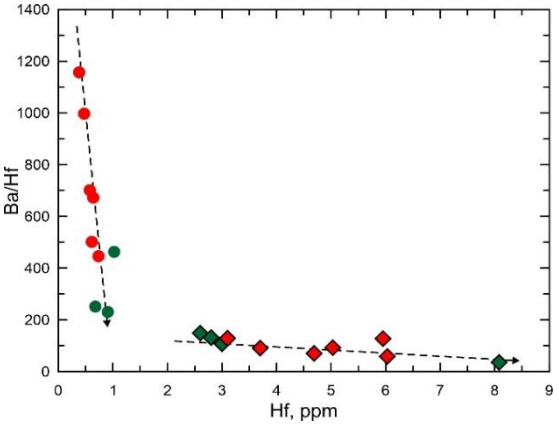

Figure 18. Hf vs Ba/Hf diagram for the Nam Meng dioritoid

The degree of partial melting also controls the total alkaline ($Na_2O + K_2O$) of the Nam Meng dioritoids. However, it shows a different tendency at low and high degrees of partial melting. At a low degree of partial melting, the total alkalinity quickly increases with the increase of partial melting. On the other hand, at the high degree of partial melting, the total alkaline slowly decreases with the increase of partial melting (Fig. 12). It suggests that the concentration of the total alkaline reaches a peak at the intermediate degree of partial melting and lower when the degree of partial melting changes.

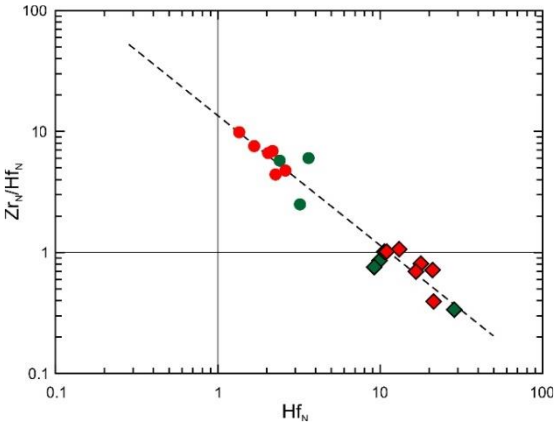

Figure 19. Logarithmic PM normalized Hf vs Zr/Hf diagram for the Nam Meng dioritoid

5. Conclusions

Based on the study of the elemental and isotope geochemistry, the formation of Nam Meng dioritoid could be concluded as follows:

(1) The Nam Meng dioritoid was derived from a magma partially melted from a spinel peridotite mantle wedge in the Indosinian subduction zone at 290 Ma. The spinel peridotite, in turn, was produced by mixing among an ancient oceanic crust, EM1, and EM2 occurred in a paleo-subduction zone at 1,258 Ma corresponding with the Meso-Neoproterozoic Rodinia supercycle.

(2) The variant in the petrographical and major oxide of the Nam Meng dioritoid was caused by the magmatic differentiation process.

(3) The variant in the LILE and HSFE of the Nam Meng dioritoid was caused by the difference in partial melting. A low degree of partial melting results in a low Hf concentration and high Ba/Hf and Zr/Hf ratios. On the other hand, a high degree of partial melting results in a high Hf concentration and low Ba/Hf and Zr/Hf ratios.

Acknowledgments

This research is granted by the Viet Nam Academy of Science and Technology's project coded NVCC11.02/22-23 and the Vietnamese state project coded DTDLCN.15/23. We thank Prof. Shinjo from the University of the Ryukyus for support with trace elements, Sr, and Nd isotope analyses. Dr. Cu Sy Thang from the Institute of Geological Sciences, Vietnam Academy of Science and Technology, for help with significant oxides analysis.

References

Boynton W.V., 1984, Cosmochemistry of the rare earth elements; meteorite studies, in Henderson, P., ed., Rare earth element geochemistry: Amsterdam, Elsevier, 63–114.

Bui P.M., Nguyen V.H., Phan V.K., Tran D.T., 2005, Geological and mineral resources map of Vietnam on 1:200.000 scale. Kim Binh - Lao Cai sheet, with Explanatory note: General Department of Geology and Minerals of Vietnam.

Chappell B.J., White A.J.R., 1974. Two Contrasting Granite Types: Pacific Geology, 8, 173–174.

Cox K.G., Bell J.D., Pankhurst R.J., 1979. The interpretation of igneous rocks, London, George, Allen and Unwin, 450p.

Goldstein S.L., O'Nions R.K., Hamilton P.J., 1984. A Sm-Nd isotopic study of atmospheric dust and particulates from major river systems: Earth and Planetary Science Letters, 70(2), 221–236.

Harker A., 1909. Natural History of Igneous Rocks, Cambridge University Press, 408p.

Hieu P.T., 2017. U-Pb zircon age of the Dien Bien granitoid in Muong Te area and their geology significance: Vietnam Journal of Geology, Series A, 363, 1–10.

Hieu P.T., Li S.-Q., Yu Y., Thanh N.X., Dung L.T., Tu V.L., Siebel W., Chen F., 2017. Stages of late Paleozoic to early Mesozoic magmatism in the Song Ma belt, NW Vietnam: evidence from zircon U-Pb geochronology and Hf isotope composition: International Journal of Earth Sciences, 106(3), 855–874.

Hoang N., 2023. Miocene - Quaternary basalts of Vietnam, Ha Noi, Publishing House for Science and Technology, 371p.

Hoang N., Uto K., 2003. Geochemistry of Cenozoic basalts in the Fukuoka district (northern Kyushu, Japan): implications for asthenosphere and lithospheric mantle interaction: Chemical Geology, 198(3–4), 249–268.

Hofmann A.W., White W.M., 1982. Mantle plumes from ancient ocean crust: Earth and Planetary Science Letters, 57(2), 421–436.

Hu Z., Gao S., 2008. Upper crustal abundances of trace elements: A revision and update: Chemical Geology, 253(3–40), 205–221.

Izokh E.P., 1971. Dien Bien Phu series, in Dovjikov A.E., ed., Geology of North Vietnam: Ha Noi, Science and Technics Publishing House, 296–320.

Jamali H., 2017. The behavior of rare-earth elements, zirconium and hafnium during magma evolution and their application in determining mineralized magmatic suites in subduction zones: Constraints from the Cenozoic belts of Iran: Ore Geology Reviews, 81, 270–279.

Johnson K.T.M., Dick H.J.B., Shimizu N., 1990. Melting in the oceanic upper mantle: An ion microprobe study of diopsides in abyssal peridotites:

Journal of the Geophysical Research, 95(B3), 2661–2678.

Kelley K.A., Plank T., Newman S., Stolper E.M., Grove T.L., Parman S., Hauri E.H., 2010. Mantle Melting as a Function of Water Content beneath the Mariana Arc: Journal of Petrology, 51(8), 1711–1738.

Kimura J.-I., Yoshida T., 2006. Contributions of Slab Fluid, Mantle Wedge and Crust to the Origin of Quaternary Lavas in the NE Japan Arc: Journal of Petrology, 47(11), 2185–2232.

Le Maitre R.W., Bateman P., Dudek A., Keller J., Lameyre M., Le Bas M.J., Sabine P.A., Schmid R., Sorensen H., Streckeisen A., Woolley A.R., Zanettin B., 1989. A Classification of Igneous Rocks and Glossary of Terms, Oxford, Blackwell Scientific Publications, 193p.

Liu J., Tran M.-D., Tang Y., Nguyen Q.-L., Tran T.-H., Wu W., Chen J., Zhang Z., Zhao Z., 2012. Permo-Triassic granitoids in the northern part of the Truong Son belt, NW Vietnam: Geochronology, geochemistry and tectonic implications: Gondwana Research, 22(2), 628–644.

McDonough W.F., Sun S.S., 1995. The composition of the Earth: Chemical Geology, 120, 223–253.

McKenzie D., Bickle M.J., 1988. The Volume and Composition of Melt Generated by Extension of the Lithosphere: Journal of Petrology, 29(3), 625–679.

McKenzie D., O'Nions R.K., 1991. Partial Melt Distributions from Inversion of Rare Earth Element Concentrations: Journal of Petrology, 32(5), 1021–1091.

Nguyen X.T., 1977. Bien Bien - Ngan Son Group, in Tran V.T., ed., Geology of Vietnam: northern part: Ha Noi, Science and Technics Publishing House, 211–219.

Pearce J.A., Harris N.B.W., Tindle A.G., 1984. Trace element discrimination diagrams for the tectonic interpretation of granitic rocks: Journal of Petrology, 25, 956–983.

Peucat J.J., Vidal P., Bernard-Griffiths J., Condie K.C., 1989. Sr, Nd, and Pb Isotopic Systematics in the Archean Low- to High-Grade Transition Zone of Southern India: Syn-Accretion vs. Post-Accretion Granulites: The Journal of Geology, 97(5), 537–549.

Phan S., Dao D.T., Nguyen D.T., Tran V.T., 2005. Geological and mineral resources map of Vietnam on 1:200.000 scale. Muong Kha - Son La sheet, with Explanatory note: General Department of Geology and Minerals of Vietnam.

Rickwood P.C., 1989. Boundary lines within petrologic diagrams which use oxides of major and minor elements: Lithos, 22, 247–263.

Rudnick R.L., Gao S., 2003. Composition of the continental crust, in Rudnick R.L., ed., The Crust, Elsevier, 31–64.

Rudnick R.L., Fountain D.M., 1995. Nature and composition of the continental crust: A lower crustal perspective: Reviews of Geophysics, 33(3), 267–309.

Shand S.J., 1943. Eruptive Rocks: Their Genesis Composition. Classification, and Their Relation to Ore-Deposits with a Chapter on Meteorite, New York, John Wiley & Sons, 444p.

Tran D.T., Dinh V.T., Nguyen D.L., Nguyen H.T., Pham V.D., Trinh T.H., 2005a. Geological and mineral resources map of Vietnam on 1:200.000 scale. Khi Su - Muong Te sheet, with Explanatory note: General Department of Geology and Minerals of Vietnam.

Tran D.T., Nguyen V.H., Pham V.D., An V.T., Nguyen B. H., 2005b. Geological and mineral resources map of Vietnam on 1:200.000 scale. Phong Sa Ly - Dien Bien Phu sheet, with Explanatory note: General Department of Geology and Minerals of Vietnam.

Tran T.A., 1994. Research on the petrology and related metallogeny of the Dien Bien and Nam Meng massifs [Bechelor: Ha Noi University, 66p.

Tran T.A., Tran T.H., Pham-Ngoc C., Shellnutt J.G., Pham T.T., Izokh E.A., Pham T.P.L., Duangpaseuth S., Soulintone O., 2022. Petrology of the Permian-Triassic granitoids in Northwest Vietnam and their relation to the amalgamation of the Indochina and Sino-Vietnam composite terranes. Vietnam J. Earth Sci., 43, 343–368.

Tran V.T., Faure M., Nguyen V.V., Bui H.H., Fyhn M.B.W., Nguyen T.Q., Lepvrier C., Thomsen T.B., Tani K., Charusiri P., 2020. Neoproterozoic to Early Triassic tectono-stratigraphic evolution of Indochina and adjacent areas: A review with new data: Journal of Asian Earth Sciences, 191, 104231.

White W.M., Hofmann A.W., 1982. Sr and Nd isotope geochemistry of oceanic basalts and mantle evolution: Nature, 296, 821–825.

Wilson M., 1989. Igneous Petrogenesis - A global tectonic approach, London, Unwin Hyman, 466p.

Zindler A., Hart S., 1986. Chemical Geodynamics: Annual Review of Earth and Planetary Sciences, 14, 493–571.